2001

# Characterisation of high temperature superconducting coils

Christopher David Cook
*University of Wollongong*, chris_cook@uow.edu.au

Sarath Perera
*University of Wollongong*, sarath@uow.edu.au

Thomas Hardjono

## Publication Details

C. David. Cook, S. Perera & T. Hardjono, "Characterisation of high temperature superconducting coils," in AUPEC2001, 2001, p. 3260331.

# Characterisation of high temperature superconducting coils

**Abstract**
Some power engineering systems, such as efficient energy storage for power quality improvement, can be potentially made more efficient if implemented with large coils made of high temperature superconductors (HTS). However, the losses of HTS coils carrying AC current limit their usage in practical applications. It has been shown previously that a thin pancake coil with relatively large diameter can be modelled as straight tapes arranged in a face-to-face stack. This paper reviews those results. In addition, measurements on a more realistic larger HTS coil were carried out. It is shown that the model assumptions provide less accurate results for a larger coil.

**Keywords**
coils, temperature, high, superconducting, characterisation

**Disciplines**
Physical Sciences and Mathematics

**Publication Details**
C. David. Cook, S. Perera & T. Hardjono, "Characterisation of high temperature superconducting coils," in AUPEC2001, 2001, p. 3260331.

# CHARACTERISATION OF HIGH TEMPERATURE SUPERCONDUCTING COILS

T. Hardono, C.D. Cook and B.S.P. Perera
School of Electrical, Computer & Telecommunications Engineering
University of Wollongong
Northfields Avenue, Wollongong, NSW 2522 Australia

**Abstract**

Some power engineering systems, such as efficient energy storage for power quality improvement, can be potentially made more efficient if implemented with large coils made of high temperature superconductors (HTS). However, the losses of HTS coils carrying AC current limit their usage in practical applications. It has been shown previously that a thin pancake coil with relatively large diameter can be modelled as straight tapes arranged in a face-to-face stack. This paper reviews those results. In addition, measurements on a more realistic larger HTS coil were carried out. It is shown that the model assumptions provide less accurate results for a larger coil.

## 1. INTRODUCTION

This paper describes the magnetic field behaviour, the critical current and the ac losses of two HTS pancake coils. The coils are prepared using Bi-2223/Ag wires. The magnetic fields of these coils are analysed using finite element methods. Predictions and measurements of the critical current of the coils will be presented including the self-field effect in the coil and the critical current results from short wires forming the coils. AC loss prediction and measurements on those coils will be presented. Electrical methods are used to measure the loss and the results are compared with the theoretical calculations.

## 2. CRITICAL CURRENTS IN HTS COILS

This section deals with the prediction of the critical current of the pancake coils based on the results from measurements on short samples from the wire. The self-field effect of the pancake will be considered in the calculation using the approximations suggested by Kim [1]. The field distribution in the coil will be calculated using finite element methods. The distribution of the transport current in the wire will also be considered. Measurements on the critical current on the coils have been carried out and the results are compared with the prediction.

### 2.1 Configurations of the wires and coils

Two pancake coils made of Bi-2223/Ag wire have been prepared, P.1 and P.2. The wires were produced at Australian Superconductors and have configurations as shown in Table 1.

P.1 was prepared using the Bi-2223/Ag wire with a total length of 6.6 m. The inner diameter of the coil is 8.2 cm and the outer diameter is 10.2 cm. The coil has 23 turns. The coil was wound manually and the layers are separated with Teflon tapes. P.2 was prepared using 100 m length of Bi-2223/Ag wire. The inner and outer diameters of the coil are 10 and 22.5 cm respectively. It has 200 turns with each layer separated by Kapton tape. Figure 1 and Table 2 provide details of the coils.

Table 1. HTS wire configurations of the pancake coils.

| Coil | Number of filaments | Width, $2d$ (mm) | Thickness, $2a$ (mm) |
|---|---|---|---|
| P.1 | 37 | 3.6 | 0.26 |
| P.2 | 27 | 3.4 | 0.27 |

### 2.2 Critical currents of the wires

The critical current of the wire has been analysed based on the measurements of short samples using the four-probe technique. Each sample of wire was 6 cm long and four taps were soldered to each sample at a distance of 1 cm apart as illustrated in Figure 2. Four samples from P.1 were measured and three measurements on each sample were carried out. Each sample *s* gives three measurements, i.e. *s*-1; *s*-2 and *s*-3 where *s* in the sample number. Therefore twelve results were obtained from the measurements as given in Table 3.

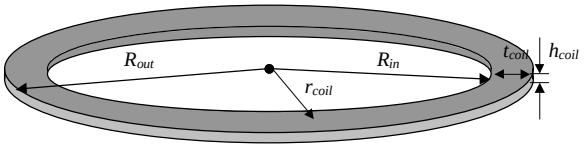


Figure 1. Configuration of pancake coil.

Table 2. Coil configurations.

| Coil | $R_{in}$ (cm) | $R_{out}$ (cm) | $r_{coil}$ (cm) | $h_{coil}$ (cm) | $t_{coil}$ (cm) | $I_c$ (A) |
|---|---|---|---|---|---|---|
| P. 1 | 4.1 | 5.1 | 4.6 | 0.4 | 1 | 18.5 |
| P. 2 | 5.0 | 11.25 | 8.125 | 0.4 | 6.25 | 5 |

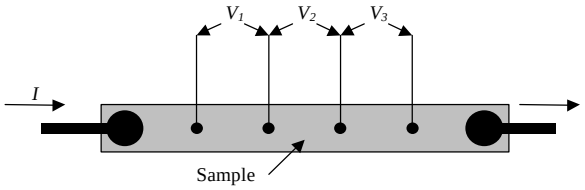


Figure 2. Configuration of sample for *I-V* measurements.

Table 3. Critical currents of short samples (P.1).

| Sample number | Critical current, $I_c$ (A) | Sample number | Critical current, $I_c$ (A) |
|---|---|---|---|
| 1-1 | 35 | 3-1 | 26 |
| 1-2 | 35 | 3-2 | 22 |
| 1-3 | 35 | 3-3 | 29 |
| 2-1 | 34 | 4-1 | 27 |
| 2-2 | 24 | 4-2 | 28 |
| 2-3 | 31 | 4-3 | 29 |

It is seen from Table 3 that the critical current of the wire varies from 22 A to 35 A. The average critical current is 29.14 A.

Critical currents of six short samples from both inner and outer side of P.2 were measured and the results are summarised in Table 4. Again, each sample *s* gives three measurements, i.e. *s*-1, *s*-2 and *s*-3 where *s* in the sample number. Sample numbers 1 to 3 are from the outer side of the coil while sample numbers 4 to 6 are from the inner side of the coil. The average value of the critical current from the outer side is 14.2 A while from the inner side is 12.8 A. The inner side samples have lower critical current ratings because they have smaller bending radius than the outer side samples. The average of all samples is 13.5 A.

Table 4. Critical currents of short samples (P.2).

| Sample number | Critical current, $I_c$ (A) | Sample number | Critical current $I_c$ (A) |
|---|---|---|---|
| 1-1 | 19.5 | 4-1 | 12.5 |
| 1-2 | 15 | 4-2 | 12.5 |
| 1-3 | 16 | 4-3 | 14 |
| 2-1 | 15.5 | 5-1 | 15 |
| 2-2 | 4 | 5-2 | 14 |
| 2-3 | 21 | 5-3 | 14.5 |
| 3-1 | 13 | 6-1 | 12.5 |
| 3-2 | 10 | 6-2 | 11.5 |
| 3-3 | 13.5 | 6-3 | 8 |
| Average $I_c$ (A) | 14.2 | Average $I_c$ (A) | 12.8 |

### 2.3 Distribution of currents in HTS wires

It is well known that transport current of an HTS wire is non-uniformly distributed across its width. When the transport current approaches the value of the critical current the distribution can be approximated using [2]:

$$\frac{I(z)}{I(z=0)} = \sqrt{1-\frac{z^2}{d^2}} \quad \text{for } -d \pounds z \pounds d \qquad (1)$$

where *I(z)* is the current per unit width at the position *z* across the wire width, *I(z=0)* is the current per unit width at the centre of the wire, and *2d* is the width of the wire.

This approximation is evident in monofilamentary wire but also valid for multifilamentary wire [2,3].

### 2.4 Finite element analysis of the coils

Figure 3 shows the distribution of the magnetic flux density on the coil surfaces along the *r*-axis of P.1 when carrying DC current. The field perpendicular to the wire cross-section is shown for different values of *z*. The parallel field is also plotted for z=0. It is seen that the perpendicular field is larger at the side of the coil. Figure 4 shows the field's distribution for P.2.

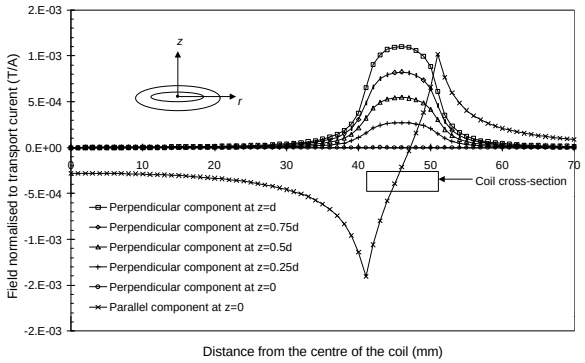


Figure 3. Field distribution at the surface of P.1 due to its transport current.

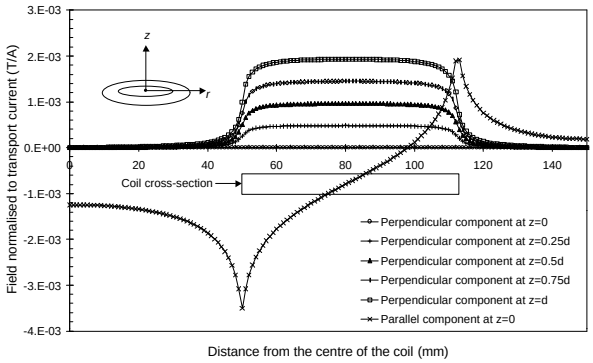


Figure 4. Field distribution at the surface of P.2 due to its transport current.

The perpendicular component of the field strength in P.2 is almost uniformly distributed along the coil surface. Its value depend on *z*, i.e. at the centre of the wire, *z*=0, the field strength is minimum and at the edge of the wire, *z=d*, it is maximum. The dependency of field strength on the *z* value is linear as can be seen in Figure 5.

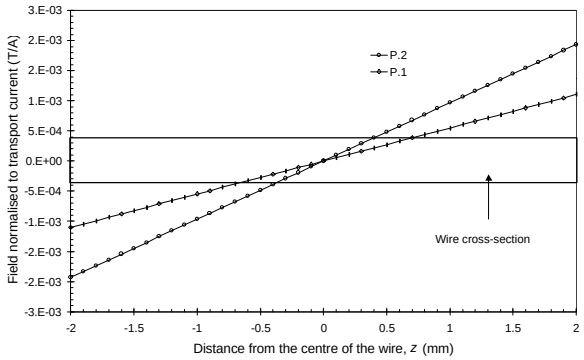


Figure 5. Field distribution along a turn at a certain radius.

### 2.5 Calculation of the critical current in coils

For a coil, based on measurements of its critical current and its self-field estimation, it is possible to work out the critical current of the wire forming the coil [4]. These methods calculate the load line for the coil based on the greatest perpendicular component of the field in the coil and apply to this the transport field performance of the wire. However, these techniques are valid for long solenoidal coils because the magnetic field at each individual turn of the winding is almost uniform across the width of the wire.

Another method was developed to calculate the field free critical current based on the critical current value of pancake coils. These methods include the effect of a non-uniform distribution of the field in the coil [2].

This section describes the calculation of the critical current of pancake coils based on the results of measurements of short samples and the self-field distribution in the coils.

The field dependency of critical current of an HTS wire can be approximated using Kim's model as:

$$\frac{I_c(B)}{I_c(0)} = \frac{1}{1+\frac{B}{B_o}} \tag{2}$$

where $I_c(B)$ is the critical current of the wire exposed to the field $B$, $I_c(0)$ is the field-free critical current of the wire, and $B_o$ is a known constant, which can be derived from curve-fitting methods from the measurement results.

It is well understood that the perpendicular component of the magnetic field causes the greatest critical current reduction of the wire [5]. Therefore in the calculation of the critical current of a pancake coil only the perpendicular component will be assessed and the parallel component will be neglected. It can also be seen in Figure 5 that the perpendicular field is linearly distributed across the width of the wire and therefore the field at position $z$ can be written as:

$$B^*_{rad}(z) = B^*_{rad}\frac{z}{d} \tag{3}$$

where $B_{rad}{}^*$ is the field normalised to transport current at $z = d$.

The critical current of the pancake coil can be calculated by solving the Kim's equation, i.e.

$$\frac{I_c(B_P,z)}{I_c(0,z)} = \frac{1}{1+\frac{B_P(z)}{B_o}} \tag{4}$$

where $B_P(z) = B^*_{rad}(z)I_c(B_P,z)$ is the self-field of the pancake coil, $B^*_{rad}(z)$ is the magnetic field normalised to transport current and $I_c(0,z)$ is the field free critical current at $z$ position.

Equation (4) can be rewritten as:

$$\frac{B^*_{rad}(z)}{B_o} I_c(B_P,z)^2 + I_c(B_P,z) - I_c(0,z) = 0 \tag{5}$$

Incorporating Equations (1) and (3) in Equation (5):

$$\frac{B^*_{rad}\frac{z}{d}\sqrt{1-\frac{z^2}{d^2}}}{B_0} I_c(B_P,z)^2 + I_c(B_P,z) - I_c(0)\sqrt{1-\frac{z^2}{d^2}} = 0 \tag{6}$$

The solution to Equation (6) is:

$$I_c(B_P,z) = \frac{-v \pm \sqrt{v^2-4uw}}{2u} \tag{7}$$

where $u = \frac{B^*_{rad}\frac{z}{d}\sqrt{1-\frac{z^2}{d^2}}}{B_0}$, $v = 1$ and $w = -I_c(0)\sqrt{1-\frac{z^2}{d^2}}$.

The critical current of the pancake coil can then be obtained by averaging the critical current for each $z$, i.e.:

$$I_c(B_P) = \frac{1}{d}\int_0^d I_c(B_P,z)dz \tag{8}$$

This approach is useful when the perpendicular component of the field is uniform along the coil cross-section. To verify these methods calculations have been made on P.2 where the perpendicular component of the self-field is almost uniformly distributed along the coil surface as shown in Figure 4. Figure 6 shows the current distribution per unit width in the wire of

the coil in the presence of its self-field compared to the field-free current per unit width of the same wire.

It can be seen that the relatively high magnetic field, i.e. at the edges of the wire, drastically reduces its critical current. Table 5 summarises the results of the calculation for P.2.

The critical current of the short wire, $I_c(0)$, a constant $B_o$ of 14 mT as discussed in Ref [2] and the field normalised to the current, $B_{rad}^*$ of 19.3 mT/A are used in Equations (7) and (8). The width of the wire is assumed to be 4 mm which is equivalent to the height of the coil.

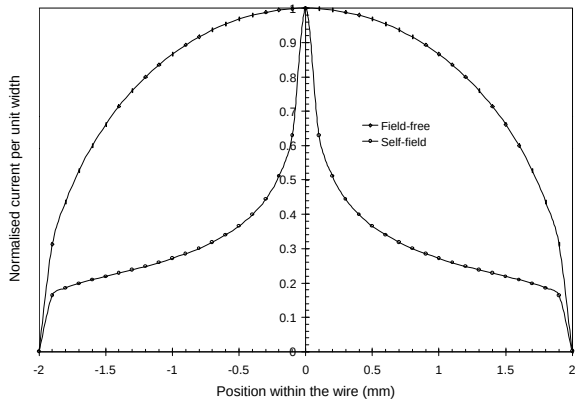


Figure 6. Current distribution in the pancake coil as a result of its self-field.

Table 5. Result from calculations of the critical current (P.2).

| $I_C(0)$ (A) | $B_o$ (mT) | $B_{rad}^*$ (mT/A) | $2d$ (mm) | $I_C(B_P)$ (A) |
|---|---|---|---|---|
| 4 (min.) | 14 | 19.3 | 4 | 2.35 |
| 21 (max.) | 14 | 19.3 | 4 | 7.27 |
| 13.5 (aver.) | 14 | 19.3 | 4 | 5.45 |

### 2.6. Measurements of the critical current in coils

The critical currents of the pancake coils have been measured using a standard transport method. The measurements were performed at the temperature of liquid Nitrogen. The critical current of P.1 is 18.5 A and that of P.2 is 5 A.

As seen from Table 5 the critical current of 5.45 for P.2 is calculated using the average of the critical current measurement results from short samples and is close to the measured value, i.e. 5 A.

## 3. AC BEHAVIOUR OF HTS COILS

This section describes the modelling and measurement of losses of coils carrying alternating current. Two pancake coils as described in Section 2 will be used. The effect of frequency on the losses will also be described.

### 3.1 Modelling of the ac losses of coils

A pancake coil with a relatively large diameter can be modelled as tapes arranged in a face-to-face stack. The configuration of this face-to-face stack is given in Figure 7. Mawatari and Müller [6,7] have shown that when the spacing $D$ is chosen to be infinitely large the loss per unit length ($P/l$) of a strip becomes that predicted by the Norris's formula for an isolated strip, i.e.:

$$\frac{P}{l} = \frac{m_o}{12p^2} w \frac{I_{pk}^4}{I_c^2} \quad \text{for } I_{pk} << I_c \tag{9}$$

and

$$\frac{P}{l} = \frac{m_o}{2p^2}(2\ln 2 - 1) w I_c^2 \quad \text{for } I_{pk} = I_c \tag{10}$$

where $I_{pk}$ is the AC peak current, $I_c$ is the DC critical current, $w$ is the angular frequency and $m_o$ is the permeability of a vacuum.

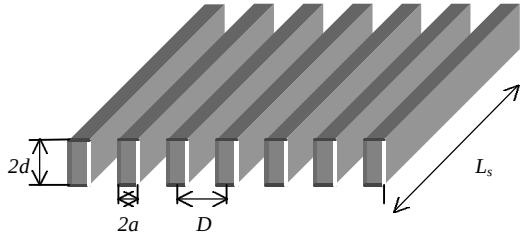


Figure 7. Face-to-face stack of HTS wires.

In contrast, when the spacing reaches its limit, $D \rightarrow 2a$, the loss per strip can be simplified to that of an infinite slab of width $2d$:

$$\frac{P}{l} = \frac{m_0}{12p} w \frac{d}{a} \frac{I_{pk}^3}{I_c} \tag{11}$$

where $d$ and $a$ are the half width and half thickness of the strip, $I_{pk}$ is the peak transport current and $I_c$ is the critical current of the strip.

### 3.2 Measurements of ac losses of the coils

For measurement of the losses in pancake coils a test-rig has been built. This incorporates a frequency generator, a bi-directional current source, a sensitive pre-amplifier, and a digital power analyser. The test set up is shown in Figure 8. The current source, connected to the frequency generator, provides sinusoidal current in the coil. The voltage at both terminals of the coil is then picked up and when

necessary amplified using the amplifier. Both the real power loss as well as the reactive power loss can be read from the power analyser.

Figure 9 presents the AC *I-V* characteristics of P.1 that was tested. The peak current varies from 0 to 60 A and the frequency was set at 50 Hz. The voltage was read from the power analyser. It can be seen that the voltage increases slightly below the critical current (18.5 A) and increases non-linearly after that value due to the flux flow properties of the coil. At higher current levels the voltage increases linearly because of the full flux flow of the coil.

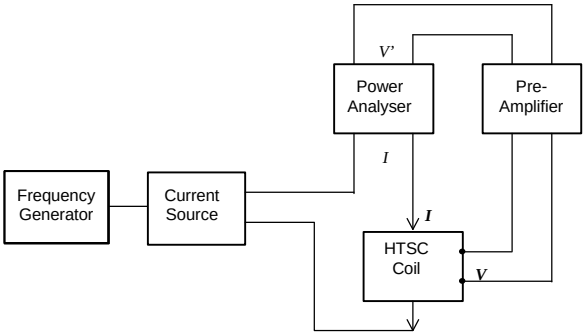


Figure 8. Set up for ac loss measurement of a pancake coil.

Figure 10 gives the results of coil losses of P.1 as a function of the AC transport current. The circles represent the measurement results. The results are compared with a theoretical calculation using Equation (11) for an infinite slab indicated with the solid line. For a peak current less than the critical one ($I_{pk}/I_c$<1) the measurement results agree well with the calculation. However, at higher currents the results tend to increase sharply above the calculated value because of greater eddy currents flowing in the coil. This work shows that the losses of the coil can be predicted using an infinite slab for a peak transport current below the DC critical current.

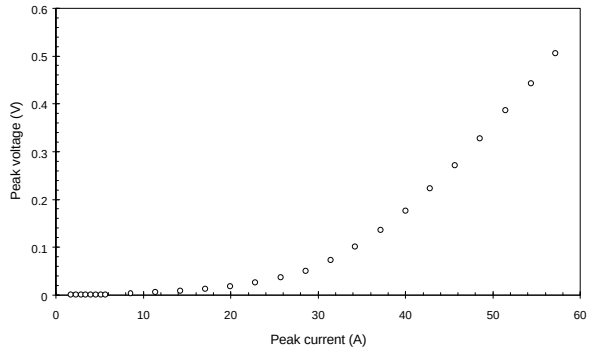


Figure 9. AC *I-V* characteristic of P.1.

For comparison the predicted losses of an isolated strip wire are also given in Figure 10. It can be concluded that the loss per unit length of wire in the form of a pancake coil is much higher than that for an isolated strip at 50 Hz.

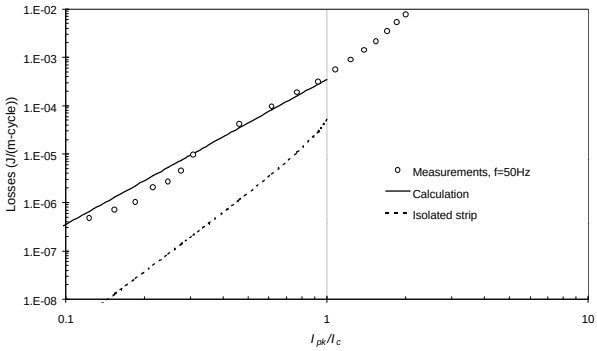


Figure 10. Losses in P.1 carrying ac transport current.

Figure 11 presents the results of AC loss tests on P.2. The inductive component of the losses was too high to measure using the power analyser when the frequency was set at 50 Hz. Therefore it was necessary to reduce the frequency. In Figure 11 the loss tests were done at two different lower frequencies, i.e. 10 Hz and 25 Hz.

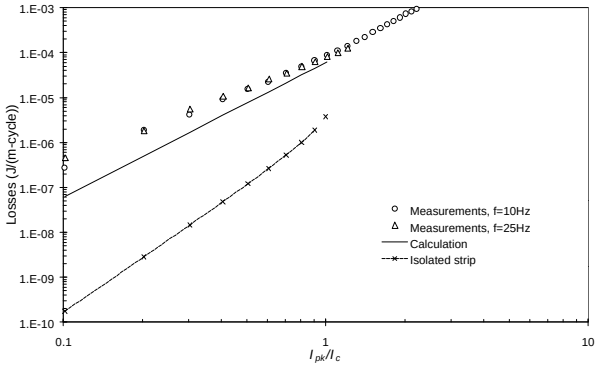


Figure 11. Losses in P.2 carrying ac transport current.

The results in Figure 11 show that for both frequencies the loss per meter per cycle agrees but the values are above that predicted by the Norris's equation for AC current far below the peak critical current. This observation shows that the calculation is less accurate for predicting the losses of a bigger coil as P.2 has an outer diameter which is much larger than the inner diameter. The ratio between the outer and inner diameter of P.2 is 2.25 compared to that of P.1, which is about 1.24, and the ratio of a face-to-face stack is 1.

When the normalised current ($I_{pk}/I_c$) is close to unity the losses approach the predicted level and above that the losses increase slightly due to eddy current effects. Again, the measurement results at both frequencies are much larger than the calculation for an isolated strip.

### 3.3 Effect of frequency on ac losses of the coils

The dependency of the coil losses on frequency for P.1 is given in Figure 12. The circles represent the coil losses for a peak current equal to 50% of the critical current ($I_{pk}$=0.5$I_c$). The diamonds represent the coil losses for $I_{pk}$=0.9$I_c$. The continuous lines are obtained by curve fitting using polynomial expressions.

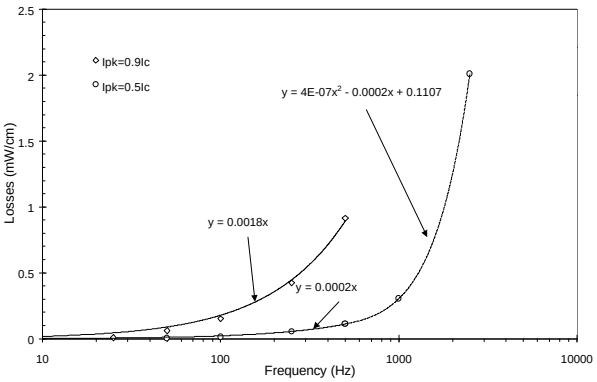


Figure 12. Frequency dependence of ac loss of P.1.

It is seen from Figure 12 that for frequencies below 500 Hz the dependency of losses on the frequency is linear. At higher frequencies the dependency is quadratic. At lower frequencies the losses are of the hysteretic type while at higher frequencies they are of the eddy current type. These results confirm the previous measurements on short wire [8].

### 4. CONCLUSIONS

Measuring the critical current of short samples obtained from the coil ends has enabled characterisation of pancake coils under DC conditions. It is shown that the average critical current of the samples provides a practical estimate for the pancake coil.

The predictions and measurement of AC loss in HTS pancake coils have also been described. It is shown that a pancake coil with relatively large diameter, eg. P.1 can be modelled as tapes arranged in a face-to-face stack. However, the measured loss in a pancake with a relatively large ratio between outer and inner diameter, eg. P.2, was above the predicted levels. The ratio of the outer and inner diameter of P.2 is 2.25 and that of P.1 is 1.24 while the ratio of a face-to-face stack is assumed to be 1.

### 5. REFERENCES


[1] Kim, Y.B., Hempstead, C.P. and Strnad, A.R., "Magnetization and Critical Supercurrents," *Physics Review*, vol. 129, pp. 528-535, 1963.

[2] Darmann, F., "Calculation of the Critical Current in Pancake-Coiled High temperature Superconducting Tapes," *Proceedings of Australasian Universities Power Engineering Conference*, Darwin, Australia, pp. 364-369, September 1999.

[3] Haken, ten, B., Eck, van, H.J.N. and Kate, ten, H.H.J., "A New Experimental Method to Determine the Local Critical Current Density in High-Temperature Superconducting Tapes," *Physica C*, vol. 334, pp. 163-167, 2000.

[4] Bodin, Z., Han, P., Vase, M., Bentzon, M.D., Skov-Hanzen, P., Bruun, R. and Goul, J., *Applied Superconductivity*, No. 2, p. 299, 1997.

[5] Ciszek, M., Tsukamoto, O., Amemiya, N., Ueyama, M. and Hayashi, K., "Angular Dependence of AC Transport Losses in Multifilamentary Bi-2223/Ag Tape on External DC Magnetic Fields," *IEEE Transactions on Applied Superconductivity*, vol. 9, no. 2, pp. 817-820, June 1999.

[6] Mawatari, Y., "Critical State of Periodically Arranged Superconducting-Strip Lines in Perpendicular Fields," *Physical Review B*, vol. 54, no. 18, pp. 13215-13221, November 1996.

[7] Müller, K.-H., "Self-Field Hysteresis Loss in Periodically Arranged Superconducting Strips," *Physica C*, vol. 289, pp. 123-130, 1997.

[8] Hardono, T., Cook, C.D. and Jin, J.X., "Performance of High Temperature Superconducting Wires and Coils for Power Engineering Applications," *Proceedings of Australasian Universities Power Engineering Conference*, Hobart, Australia, pp. 86-90, September 1998.